Electron beam properties in self-modulated laser wakefield acceleration using TW and sub-TW pulses

Edison Puig Maldonado
Instituto Tecnológico de Aeronáutica
São José dos Campos, SP, Brazil
puig@ita.br

Ricardo Elgul Samad
IPEN-CNEN/SP
São Paulo, SP, Brazil
resamad@gmail.com

Alexandre Bonatto
Universidade Federal de Ciências da Saúde,
Porto Alegre, RS, Brazil
abonatto@ufcspa.edu.br

Roger Pizzato Nunes
Universidade Federal do Rio Grande do Sul,
Porto Alegre, RS, Brazil
roger.pizzato@ufrgs.br

Sudeep Banerjee
Arizona State University,
Tempe, AZ, USA
sudeep.banerjee@asu.edu

Nilson Dias Vieira Junior
IPEN-CNEN/SP
São Paulo, SP, Brazil
nilsondiasvieirajr@gmail.com

2021 SBFoton International Optics and Photonics Conference (SBFoton IOPC) | 978-1-6654-1948-2/21/$31.00 ©2021 IEEE | DOI: 10.1109/SBFOTONIOPC50774.2021.9461971

***Abstract*— We review the fundamentals of electron beam generation in self-modulated laser wakefield acceleration (SM-LWFA) using laser pulses with peak powers on the TW and sub-TW scale. The results of several new particle-in-cell simulations for λ = 0.8 μm and a thin H_2 gas target are shown. By scanning the peak gas density and peak power values of the incident laser, we discuss the resulting acceleration processes, as well as the characteristics of the electron beams generated for different conditions. Our approach provides a method to optimize these beams with lasers operating at kHz repetition rates.**

Keywords — High-power lasers and high-field phenomena, laser wakefield acceleration, particle-in-cell, plasma simulation, particle beam simulation.

I. Introduction

Electron beams of subpicosecond duration and up to GeV energy can now be generated by *laser wakefield acceleration*, LWFA [1, 2]. Typically, the leading edge of an intense ultrashort laser pulse causes field-induced ionization in a neutral gas target and the pulse excites a high-amplitude, nonlinear wakefield as it propagates through the generated plasma. Background electrons can be trapped within this wakefield, being pushed by strong local electric fields [3, 4]. The acceleration field in these systems can be up to TV/m [5], 10^4 times stronger than those of superconducting radio-frequency acceleration cavities. This allows the production of high-energy bunched electron beams in compact systems with interaction length in the scale of centimeters [1, 5]. Researchers are currently exploring the production of even stronger wakefields to generate 10 GeV electrons and beyond [6, 7].

LWFA has allowed new applications such as compact, tunable, ultrafast, high-energy (ionizing) radiation sources, which can be used in new imaging techniques [8, 9]. However, increasing the repetition rate of the accelerated beams to the kHz is a requirement for many applications, such as those in which scanning and/or data collection statistics are required [10, 11], in imaging, matter probing and isotope production [5, 12, 13]. Operation at kHz in the so-called *blowout* LWFA regime requires complex laser systems providing few fs (few optical cycles) laser pulses with peak power around TW [14-17]. On the other hand, operation in the self-modulated LWFA regime, SM-LWFA [18], allows the use of simpler tabletop laser systems [19, 20], which can provide pulses of ~ 100 fs with peak power of tenths of TW at kHz repetition rate [21, 22]. In this regime, the laser self-focusing effect produces a near diffraction limited spot, enhancing the self-modulation phenomenon and, when self-channeling is achieved, acceleration of a multi-MeV bunched electron beam can be obtained. Although these accelerated electrons have a broader energy spectrum and greater divergence than those generated by the blowout regime, the full accelerated charge per shot can be two orders of magnitude higher [3, 22]. Moreover, for specific SM-LWFA configurations, *quasimonoenergetic* electron bunches can be obtained as a minor part (of less than 1%) of the electrons in the beam [23, 24], with characteristics similar to those obtained from the *blowout* LWFA systems operating at kHz [24-26].

SM-LWFA with sub-TW laser pulses requires very dense and thin (sub-mm) targets, as demonstrated in its first successful achievement [25], which used a H_2 gas flow. For operating at kHz repetition rates, both mentioned techniques require plasma targets with densities around a few tenths of the critical value (for laser-plasma interaction) and thicknesses of a few hundred microns, with continuous flow [27] or driven by fast valves. By using pure H_2, the optical field-induced ionization fully saturates for intensities as low as 10^{14} W/cm^2 [22, 28]. In such gas jets, usually with Mach number from 1 to 6, reaching the necessary densities requires backing pressures in the range of 10-1000 bar and, in some cases, cryogenic cooling [29-31].

In this work, quasi-3D particle-in-cell simulations (PIC) were performed, as well as analyses to characterize the dynamics of processes and accelerated beams. We discuss the SM-LWFA using TW and sub-TW laser pulses, starting with a parameter scan. Peak laser powers from 0.25 to 4 TW were considered and a range of plasma densities was examined: the lower limit leads to the relativistic self-focusing and the upper limit is ~60% of the critical plasma density. The main characteristics of the accelerated electron beams were determined, such as duration, charge, energy distribution, and beam emittance.

II. Basics of blowout LWFA and SM-LWFA

A laser pulse with angular frequency ω and duration τ_0 travels in a plasma with electron density, n_e, below the critical value (thus, an *underdense* plasma), $n_e < \epsilon_0 m_e (\omega/e)^2 \equiv n_{cr}$, where ϵ_0 is the vacuum permittivity, m_e is the relativistic electron mass, e is the elementary charge. The *plasma frequency*, $\omega_p = (e/\epsilon_0^{1/2}) \times (n_e/m_e)^{1/2}$, defines the laser phase velocity, $v_p = c / [1 - (\omega_p/\omega)^2]^{1/2}$, and the laser group velocity, $v_g = c \times [1 - (\omega_p/\omega)^2]^{1/2}$, where c is the speed of light in vacuum. Through the ponderomotive force, the laser pulse excites oscillations at ω_p, so that its propagation is followed by a plasma wake, with wavelength $\lambda_p \approx 2\pi c/\omega_p$. When the dimensionless laser amplitude, a_0, is above unity, $a_0 \equiv eE_0/(\omega m_e c) > 1$, where E_0 is the laser electric field peak amplitude, this wakefield starts to present ion cavities with a sawtooth-like longitudinal electric field [3]. Background electrons can be trapped in these ion cavities, e.g., aided by a wave breaking event [3, 32].

This work was supported by FAPESP.

978-0-7381-2418-6/21/$31.00 ©2021 IEEE

If the plasma density is adjusted so that $c\tau_0 \lesssim \lambda_p/2$ and the laser beam diameter is close to λ_p, a wakefield with near spherical cavities can be generated. This allows operation in the *blowout* regime [3] and, therefore, the acceleration of quasimonoenergetic electrons, as long as the laser meets the usual criteria that its peak power, P_L, exceeds the critical power, $P_c^{(b)}$, where [33]:

$$P_c^{(b)}\,[\mathrm{GW}] = 30\,(\tau_0\,[\mathrm{fs}] / \lambda\,[\mu\mathrm{m}])^2. \quad (1)$$

When using the tabletop laser systems mentioned above, with pulses of ~ 100 fs and peak power of tenths of TW, this condition is not attainable. An alternative is to operate in the *self-modulated laser wakefield acceleration* regime, SM-LWFA, conceived in the early 1990s [18, 34], as long as the plasma density is now readjusted so that the peak laser power exceeds the *critical power for self-focusing*:

$$P_c\,[\mathrm{GW}] = 17\,(n_{cr}/n_e). \quad (2)$$

Then, variations in plasma density in the wakefield modulate the laser pulse, which evolves into fragments of the envelope that now resonate with it. Due to the short dephasing length, $L_d = \lambda_P{}^3/2\lambda^2$, and to the limited extent that the self-focusing balances the diffraction, thin targets are often used [3, 25].

There are three distinct operating ranges for SM-LWFA (or sub-regimes) [35]. Referring to the position of maximum laser amplitude after self-focusing, z', the first range of parameters causes it to occur in a low-density region. The laser undergoes moderate self-modulation and a low-charge electron beam is obtained. In the second range of parameters, z' occurs in a region with high enough density, leading to a strong self-modulation of the laser, followed by self-channeling [3, 36], and a beam of electrons with a higher charge and energy is produced. The third parameter range is associated with denser plasmas (close to the critical value), with shorter dephasing lengths, and a beam of lesser quality in energy and divergence is generated [37].

In SM-LWFA, the energy gain can also be assisted [38] by a resonant interaction between the electron oscillation within the ion cavity and the laser magnetic field. This phenomenon is called *direct laser acceleration*, DLA [39] and depends on the pulse-wake superposition parameter $T_p = c\tau_L/\Lambda_{wake}$, where τ_L is the laser fragment duration and $\Lambda_{wake} = (a_0)^{1/2}\lambda_p$ is the nonlinear plasma wavelength [40, 41].

III. Methods

All simulations were performed in a desktop PC running Linux, using the quasi-cylindrical (quasi-3D), Fourier-Bessel Particle-In-Cell code, FBPIC, originally developed by Remi Lehe at Lawrence Berkeley National Laboratory and Manuel Kirchen at CFEL, Hamburg University [42]. The local density of plasma electrons is calculated from the neutral gas using the Ammosov-Delone-Krainov ionization model (ADK) [43]. In the simulations, the volume evaluated at each step has radius $R = 20$ μm and length $\Delta z = 60$ μm. The spectral calculation is performed considering three azimuthal modes. Fields are evaluated in a grid that has 2250 points in Δz and 400 points in R, a density that corresponds to 30 points/λ, in the longitudinal direction, and 30 points/w_{min}, in the radial direction (estimating an approximate value for the minimum laser beamwaist $w_{min} \approx 1.5$ μm). The number of particles per cell (ppc) is 2 along z, 2 along r and 12 along θ, following the developer recommendation [44].

We considered the target as a jet of H_2 gas flowing in the y direction, with a diameter of 200 μm in the laser path. The laser pulse propagates in the z direction and crosses the center of the target (the jet axis). The H_2 gas density has a radial profile with a linear ascending ramp of 80 μm and a central plateau, therefore, a trapezoidal profile with 120 μm FWHM, in a diametrical cut. This is a good representation for the flow from a submillimetric supersonic nozzle [45, 46]. The background is assumed to be absolute vacuum. When all hydrogen in the cross section of the laser is ionized, the local plasma electron density on the plateau is n_{e0}. The main laser and plasma parameters used in the simulations are shown in Table I. The relevant computing parameters are shown in Table II. Each simulation took 25-50 hours to complete.

The laser pulse starts at $z = 0$ μm and is linearly polarized in the x direction. The laser beam, considered ideal Gaussian with $M^2 = 1$, is focused on vacuum (without the target) at $z = 50$ μm to $w_0 = 7$ μm. The general configuration is similar to that found in the first SM-LWFA experiments using sub-TW laser pulses [22, 25]. Although electrons of all energies are considered in the execution of the simulations, only those with $u_z \geq m_0 c$ (energies above 0.21 MeV) were considered in the electron beam analyses.

TABLE I. Laser and plasma parameters used in the simulations. Asterisk values are the independent input data. MIV: measured in vacuum. Values of I_0 and a_0 are at the vacuum propagating beam focus position. The gas and plasma parameters shown are referred to the density plateau.

PHYSICAL PARAMETER	VALUE
Laser, initial pulse duration, τ_0 (fs)	50
Laser, initial peak power, P_L (TW)	¼, ½, 1, 2, 4
* Laser, wavelength, λ (μm)	0.8
* Laser, pulse center start position, z_0 (μm)	0
* Laser (MIV), pulse length (FWHM), $L_0 = c\tau_0$ (μm)	15
* Laser (MIV), focus position, z_{foc} (μm)	50
* Laser (MIV), beamwaist, w_0 (μm)	7.0
* Laser (MIV), dimensionless amplitude, a_0	0.4 to 1.6
Laser (MIV), Rayleigh range, z_R (μm)	192
Laser (MIV), intensity, I_0 (10^{17} W cm^{-2})	3 to 50
* Target, species (gas)	H_2
* Target, top atomic density, n_{atoms} (10^{19} cm^{-3})	1 to 100
* Target, start position in z (μm)	0
* Target, total z-extension (μm)	200
* Target, length of entry and exit ramps (μm)	80
Plasma, wavelength, λ_p (μm)	1 to 10.5
Plasma, dephasing length, L_d (μm)	1 to 912
Plasma, group velocity (v_g/c)	0.65 to 1

TABLE II. Computing parameters used in the simulations. The number of particles per cell is 2 along z, 2 along r and 12 along θ.

SIMULATION PARAMETER	VALUE
Start position of the simulation box (μm)	-20
Simulation box length, Δz (μm)	60
Simulation box diameter, $2R$ (μm)	40
Number of grid points along z	2250
Number of grid points along r	400
Number of azimuthal modes, n_m	3
Number of particles per cell	48
Speed of the moving window, v_w (c)	0.8 to 1
Simulation timestep, Δt (as)	89
Simulation length, maximum (μm)	290

IV. RESULTS

Next, to identify each simulated configuration, the notation $\{P_L\,(\mathrm{TW}),\ n_{e,0}\,(10^{20}\,\mathrm{cm}^{-3})\}$ is adopted. In all simulations, the position in which self-modulation produces the shortest laser pulse fragments is also z' (the point of maximum laser amplitude). A nonlinear wakefield is excited when the laser pulse approaches z'.

In the *first range* of simulation parameters, z' occurred around the middle of the target exit ramp. The following studied configurations are within this range: $\{¼, <5\}$, $\{½, <2\}$, $\{1, <1\}$, $\{2, <0.5\}$ and $\{4, <0.3\}$. The common characteristics observed are: (1) there was no observable self-channeling; (2) laser pulse fragments had a superposition of $0.8 \lesssim T_p < 2$; (3) the accelerated pulsed beam was formed by bunches, with a total duration of a few tens of fs and low divergence; (4) under the same laser peak power, the maximum electron energy increased with the plasma density.

In the *second parameter range*, simulations showed z' near the end of the density plateau, with subsequent laser self-channeling. The optimum acceleration results were obtained here. Configurations classified in this range are: $\{½, 2 \text{ to } 3\}$, $\{1, 1 \text{ to } 3\}$, $\{2, 0.5 \text{ to } 3\}$ and $\{4, 0.3 \text{ to } 2\}$. The other characteristics verified in this case are: (1) laser pulse fragments presented superposition parameter in the range of $0.3 \lesssim T_p < 1$; (2) the pulsed electron beams had a typical duration of a few tens of fs and moderate divergence; (3) quasimonoenergetic bunches occurred, presenting a much shorter duration of a few fs.

In the *third parameter range*, the positions z' occurred in the first half of the target (due to the higher plateau density values). The following studied configurations are in this range: $\{¼, \gtrsim 5\}$, $\{½, >3\}$, $\{1, >3\}$, $\{2, >3\}$ and $\{4, >2\}$. Characteristics obtained: (1) there was no self-channeling and the short dephasing length restricted the acceleration process to a few microns in z; (2) $T_p \lesssim 1$; (3) the pulsed electron beams had duration of several tens of fs and higher divergence; (4) under the same initial laser peak power, the maximum electron energy decreased with the plasma density.

A simulation using $P_L = 0.5$ TW, with $a_0 \approx 0.6$ (in vacuum), and peak density $n_{e,0} = 2\times10^{20}$ cm^{-3} ($\sim 0.11\ n_{cr}$) is now discussed as a representative case of the processes within the *second parameter range*. The evolution of the axial laser pulse envelope is shown in Fig. 1, as the as dimensionless amplitude, a_0. With $z' \approx 135$ µm, the new laser amplitude is $a_0' \approx 1.6$, and the main fragment length is $L_0' \approx 1$ µm. The local superposition parameter is $T_p \approx 0.4$.

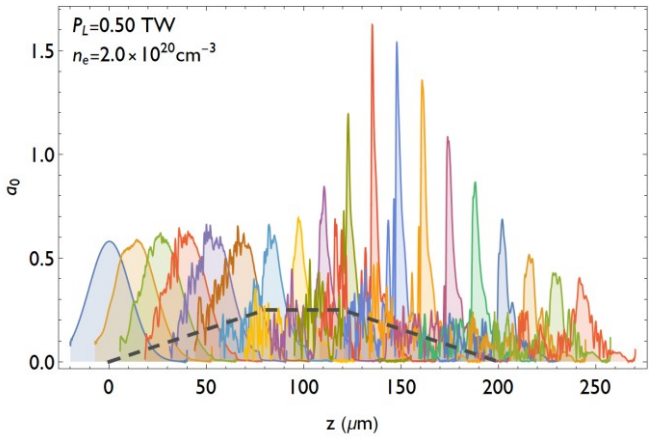

Fig. 1. Plots of the on-axis laser pulse envelope, as a function of z, obtained at different simulation times, for the $\{0.5, 2\}$ simulation. The dotted line is a guide for the eye, without scale, that represents the target density profile.

Trapped electrons are accelerated along an extension that corresponds to most of the downramp, although the nominal dephasing length is only $L_d \approx 10$ µm on the target plateau. Fig. 2(a) and (b) show two x-z cross-sections of the charge density field: (a) the nonlinear wakefield, when in the middle of the downramp, (b) the electrons leaving the target at a later time. The bunch on the right, at $z \approx 227$ µm, is quasimonoenergetic and has normalized rms emittances: $\varepsilon_{x,rms} \approx 0.5$ mm mrad and $\varepsilon_{y,rms} \approx 0.8$ mm mrad.

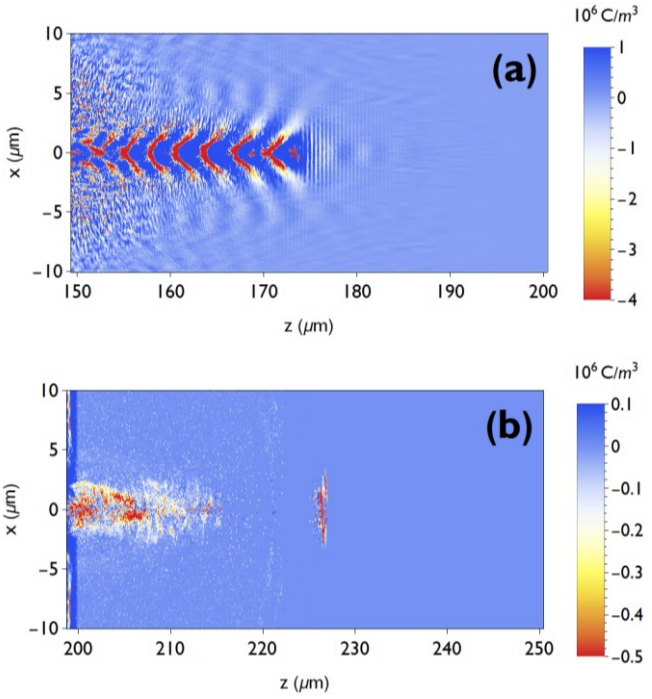

Fig. 2. Two snapshots of the electric charge density field cross section in a cut in the x-z plane, $\rho(x, z)$, obtained from the simulation with $P_L = ½$ TW ($a_0 \approx 0.6$) and target peak electron density $n_{e,0} = 2\times10^{20}$ cm^{-3}. The color scales are saturated in both plots, the full-scale values are [-13, 1.7]×10^7 C/m^3 in (a), and [-8.8, 0.2]×10^6 C/m^3 in (b).

Fig. 3 shows the energy distributions of the electrons that have just left the target, for representative configurations in each of the three parameter ranges. They are composed by quasi-exponential Maxwellian distributions, with median energies of 0.63 MeV in (a), 0.92 MeV in (b) and 0.61 MeV in (c). It is noticeable that case (b) also presents a quasimonoenergetic peak at 8.9 MeV, with a width (FWHM) of 1.2 MeV, exclusively associated with the isolated and advanced bunch in Fig. 2 (b).

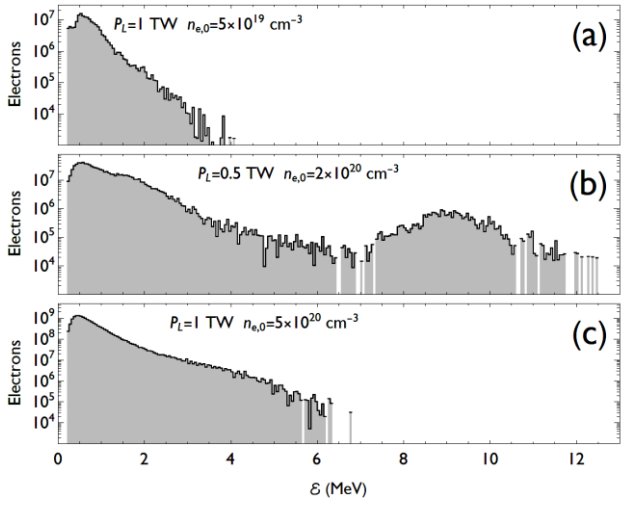

Fig. 3. Energy distributions of the accelerated beams, right after the electrons leave the target, obtained from simulations: (a) $P_L = 1.0$ TW ($a_0 \approx 0.8$) and peak density $n_{e,0} = 5\times10^{19}$ cm^{-3}, (b) $P_L = ½$ TW ($a_0 \approx 0.6$) and peak density $n_{e,0} = 2\times10^{20}$ cm^{-3}, and (c) $P_L = 1$ TW ($a_0 \approx 0.8$) and peak density $n_{e,0} = 5\times10^{20}$ cm^{-3}. The histograms have 250 bins over the range.

Fig. 4 to Fig. 7 show the calculated values for the main parameters of all electron beams obtained (considered immediately after leaving the target), as a function of the plasma density on the plateau and the incident laser peak power. Fig. 4 presents a plot of the total charge, Q_T (absolute value), which, as a general trend, grows with n_{e0}. We defined a reference kinetic energy for the electrons as its median value, $\tilde{K}$, which show a peak around 2×10^{20} cm^{-3}, as presented in Fig. 5. The maximum values of kinetic energy obtained for the electrons, K_{max}, are presented in Fig. 6, with peaks occurring from 1×10^{20} cm^{-3} to 5×10^{20} cm^{-3}. Fig. 7 shows the calculated normalized transverse rms emittances, ranging from a few tenths to several tens, increasing with the plasma density. All these parameter values obtained also increase with the laser peak power, as a general trend.

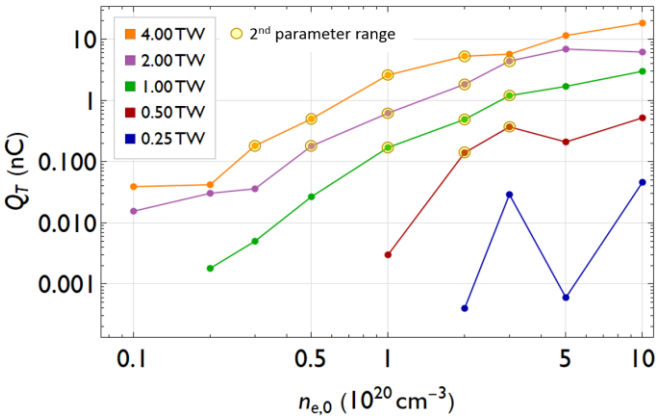

Fig. 4. Total charge of the electrons leaving the target, as a function of the peak plasma density, for each incident laser peak power.

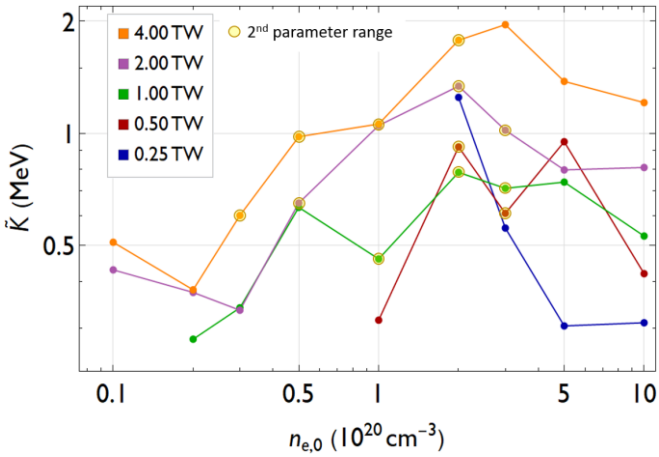

Fig. 5. Reference energy (median) of the electrons leaving the target, as a function of the peak plasma density, for each incident laser peak power.

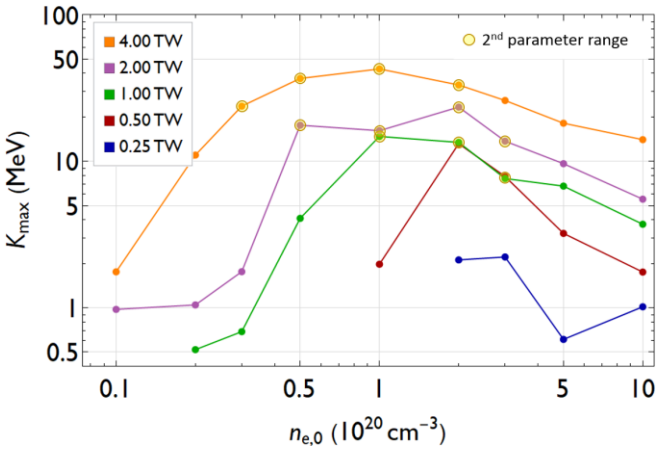

Fig. 6. Maximum energy of the electrons leaving the target, as a function of the peak plasma density, for each incident laser peak power.

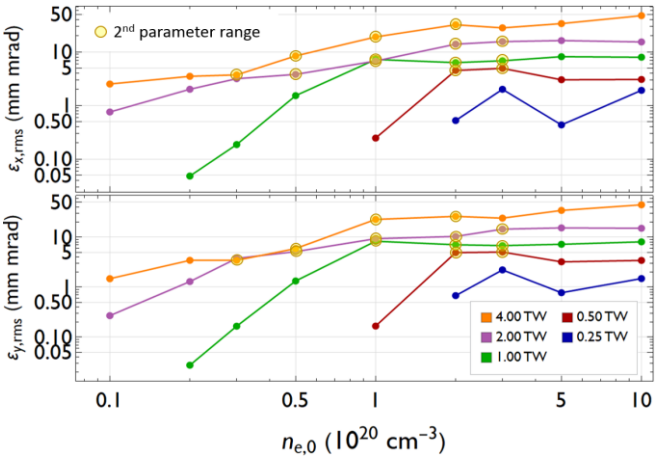

Fig. 7. Normalized transverse *rms* emittances of all electrons leaving the target, in the *x* (upper graph) and *y* (lower graph) directions, as functions of the peak plasma density, for each incident laser peak power.

V. Discussion and Conclusions

In this original study of SM-LWFA regimes using TW and sub-TW laser pulses, sweeping a wide range of parameters, the generated electron beams were compared in terms of charge, energy, and emittance, allowing for a better assessment of each process. In general, the accelerated beam presented predominant quasi-exponential spectrum, with median energy values around 1 MeV. When the maximum laser intensity occurred at a position near the end of the density plateau (which we classify as operation in the *second parameter range*), the subsequent laser self-channeling led to a continuous wakefield along the downramp, and the highest electron energies were obtained. Our results indicated maximum energy values of 5-50 MeV, and the simulations of this sub-regime were prone to generate quasimonoenergetic bunches. The normalized transverse rms emittances ranged from a fraction of mm mrad in the first parameter range (a few mm mrad for 2-4 TW) to up to several mm mrad in the third parameter range (tens of mm mrad for 2-4TW). In the {¼, 5} simulation, the low values obtained are not reproduced in higher resolution simulations performed on a supercomputer; therefore, they can be a mathematical artifact related to this range of values in this simulation resolution. The values for the other configurations show good correspondence with those of the supercomputer.

Summary – In this paper, we review the fundamentals of SM-LWFA using TW and sub-TW laser pulses and analyzed the results of a set of PIC simulations, considering a general setup close to that of important experimental demonstrations. The characteristics of the processes obtained as a function of the main laser and plasma parameters were discussed and classified into three sub-regimes. The results are in accordance with the reference values obtained experimentally, reported by other groups [25] and with the expected trends for SM-LWFA [35]. The accelerated electron beams obtained in configurations of up to 1 TW have charge, energy and emittance values that make them relevant for applications where a high dose of radiation is required [37, 47, 48], in systems operating at a repetition rate of kHz.

Acknowledgment

We would like to thank FAPESP for the grant in the Program "São Paulo Researchers in International Collaboration, SPRINT", Process 2018/25961-7.

References

[1] T. Tajima, K. Nakajima, and G. Mourou, "Laser Acceleration," *Riv. del Nuovo Cim.*, vol. 40, no. 2, pp. 33–133, 2017.

[2] V. Malka, "Laser plasma accelerators," *Phys. Plasmas*, vol. 19, no. 5, p. 055501, May 2012.

[3] E. Esarey, C. B. Schroeder, and W. P. Leemans, "Physics of laser-driven plasma-based electron accelerators," *Rev. Mod. Phys*., vol. 81, no. 3, pp. 1229–1285, 2009.

[4] S. M. Hooker, "Developments in laser-driven plasma accelerators," *Nat. Photonics*, vol. 7, no. 10, pp. 775–782, 2013.

[5] B. Hidding et al., "Plasma Wakefield Accelerator Research 2019 - 2040: A community-driven UK roadmap compiled by the Plasma Wakefield Accelerator Steering Committee (PWASC)," 2019.

[6] W. P. Leemans *et al.*, "Multi-GeV Electron Beams from Capillary-Discharge-Guided Subpetawatt Laser Pulses in the Self-Trapping Regime," *Phys. Rev. Lett*., vol. 113, no. 24, p. 245002, Dec. 2014.

[7] A. J. Gonsalves et al., "Petawatt Laser Guiding and Electron Beam Acceleration to 8 GeV in a Laser-Heated Capillary Discharge Waveguide," *Phys. Rev. Lett.*, vol. 122, no. 8, p. 084801, Feb. 2019.

[8] A. Giulietti and T. Tajima, *Laser-Driven Particle Acceleration Towards Radiobiology and Medicine*. Cham: Springer International Publishing, 2016.

[9] F. Albert, "Next-Generation Light Sources: Laser Wakefield Accelerators," *Opt. Photonics News*, January, pp. 42–49, 2018.

[10] R. Polanek *et al.*, "1 kHz laser accelerated electron beam feasible for radiotherapy uses: A PIC–Monte Carlo based study," *Nucl. Instruments Methods Phys. Res. Sect. A Accel. Spectrometers, Detect. Assoc. Equip.*, vol. 987, no. October 2020, p. 164841, Jan. 2021.

[11] J. Faure, B. van der Geer, B. Beaurepaire, G. Gallé, A. Vernier, and A. Lifschitz, "Concept of a laser-plasma-based electron source for sub-10-fs electron diffraction," *Phys. Rev. Accel. Beams*, vol. 19, no. 2, p. 021302, Feb. 2016.

[12] Z.-H. He *et al.*, "Capturing Structural Dynamics in Crystalline Silicon Using Chirped Electrons from a Laser Wakefield Accelerator," *Sci. Rep.*, vol. 6, no. 1, p. 36224, Dec. 2016.

[13] F. Albert and A. G. R. Thomas, "Applications of laser wakefield accelerator-based light sources," *Plasma Phys. Control. Fusion*, vol. 58, no. 10, p. 103001, Nov. 2016.

[14] D. Guénot *et al.*, "Relativistic electron beams driven by kHz single-cycle light pulses," *Nat. Photonics*, vol. 11, no. 5, pp. 293–296, May 2017.

[15] D. Gustas *et al.*, "High-charge relativistic electron bunches from a kHz laser-plasma accelerator," *Phys. Rev. Accel. Beams*, vol. 21, no. 1, p. 013401, Jan. 2018.

[16] J. Faure *et al.*, "A review of recent progress on laser-plasma acceleration at kHz repetition rate," *Plasma Phys. Control. Fusion*, vol. 61, no. 1, p. 014012, Jan. 2019.

[17] F. Salehi, M. Le, L. Railing, and H. M. Milchberg, "Laser-accelerated, low divergence 15 MeV quasi-monoenergetic electron bunches at 1 kHz," *arXiv e-prints*, no. oct, p. arXiv:2010.15720, Oct. 2020.

[18] J. Krall, A. Ting, E. Esarey, and P. Sprangle, "Enhanced acceleration in a self-modulated-laser wake-field accelerator," *Phys. Rev. E*, vol. 48, no. 3, pp. 2157–2161, Sep. 1993.

[19] H. Fattahi *et al.*, "Third-generation femtosecond technology," *Optica*, vol. 1, no. 1, p. 45, Jul. 2014.

[20] J. Henrich, S. Butcher, and M. Arrigoni, "Ultrafast Lasers: Trends in femtosecond amplifiers - Ti:sapphire vs. ytterbium," *Laser Focus World*, no. Feb 18th, pp. 1–7, 2020.

[21] Z.-H. He *et al.*, "High repetition-rate wakefield electron source generated by few-millijoule, 30 fs laser pulses on a density downramp," *New J. Phys.*, vol. 15, no. 5, p. 053016, May 2013.

[22] F. Salehi *et al.*, "MeV electron acceleration at 1 kHz with <10 mJ laser pulses," *Opt. Lett.*, vol. 42, no. 2, p. 215, Jan. 2017.

[23] B. Hidding *et al.*, "Generation of Quasimonoenergetic Electron Bunches with 80-fs Laser Pulses," *Phys. Rev. Lett.*, vol. 96, no. 10, p. 105004, Mar. 2006.

[24] M. Mori *et al.*, "Transverse dynamics and energy tuning of fast electrons generated in sub-relativistic intensity laser pulse interaction with plasmas," *Phys. Lett. A*, vol. 356, no. 2, pp. 146–151, Jul. 2006.

[25] A. J. Goers *et al.*, "Multi-MeV Electron Acceleration by Subterawatt Laser Pulses," *Phys. Rev. Lett.*, vol. 115, no. 19, p. 194802, Nov. 2015.

[26] M.-W. Lin *et al.*, "Laser wakefield acceleration driven by a few-terawatt laser pulse in a sub-mm nitrogen gas jet," *Phys. Plasmas*, vol. 27, no. 11, p. 113102, Nov. 2020.

[27] Z.-H. He *et al.*, "Electron diffraction using ultrafast electron bunches from a laser-wakefield accelerator at kHz repetition rate," *Appl. Phys. Lett.*, vol. 102, no. 6, p. 064104, Feb. 2013.

[28] H. Ekerfelt, "Numerical and Experimental Studies of Wakefield Accelerators," Lund University, 2019.

[29] S. Semushin and V. Malka, "High density gas jet nozzle design for laser target production," *Rev. Sci. Instrum.*, vol. 72, no. 7, pp. 2961–2965, Jul. 2001.

[30] J. L. Henares *et al.*, "Development of gas jet targets for laser-plasma experiments at near-critical density," *Rev. Sci. Instrum.*, vol. 90, no. 6, p. 063302, Jun. 2019.

[31] F. Salehi, A. J. Goers, L. Feder, B. Miao, D. Woodbury, and H. M. Milchberg, "Characterization of a 100 micrometer-scale cryogenically cooled gas jet for near-critical density laser-plasma experiments," *Rev. Sci. Instrum.*, vol. 90, no. 10, p. 103001, Oct. 2019.

[32] S. V. Bulanov *et al.*, "Electron bunch acceleration in the wake wave breaking regime," *Plasma Phys. Reports*, vol. 32, no. 4, pp. 263–281, Apr. 2006.

[33] S. Gordienko and A. Pukhov, "Scalings for ultrarelativistic laser plasmas and quasimonoenergetic electrons," *Phys. Plasmas*, vol. 12, no. 4, p. 043109, Apr. 2005.

[34] K. Nakajima *et al.*, "Observation of Ultrahigh Gradient Electron Acceleration by a Self-Modulated Intense Short Laser Pulse," *Phys. Rev. Lett.*, vol. 74, no. 22, pp. 4428–4431, May 1995.

[35] D. Woodbury *et al.*, "Laser wakefield acceleration with mid-IR laser pulses," *Opt. Lett.*, vol. 43, no. 5, p. 1131, Mar. 2018.

[36] S.-Y. Chen, M. Krishnan, A. Maksimchuk, R. Wagner, and D. Umstadter, "Detailed dynamics of electron beams self-trapped and accelerated in a self-modulated laser wakefield," *Phys. Plasmas*, vol. 6, no. 12, pp. 4739–4749, Dec. 1999.

[37] B. S. Nicks, T. Tajima, D. Roa, A. Nečas, and G. Mourou, "Laser-wakefield application to oncology," *Int. J. Mod. Phys. A*, vol. 34, no. 34, p. 1943016, Dec. 2019.

[38] N. Lemos *et al.*, "Self-modulated laser wakefield accelerators as x-ray sources," *Plasma Phys. Control. Fusion*, vol. 58, no. 3, p. 034018, Mar. 2016.

[39] A. Pukhov, Z.-M. Sheng, and J. Meyer-ter-Vehn, "Particle acceleration in relativistic laser channels," *Phys. Plasmas*, vol. 6, no. 7, pp. 2847–2854, Jul. 1999.

[40] C. B. Schroeder and E. Esarey, "Relativistic warm plasma theory of nonlinear laser-driven electron plasma waves," *Phys. Rev. E*, vol. 81, no. 5, p. 056403, May 2010.

[41] J. L. Shaw, N. Lemos, K. A. Marsh, D. H. Froula, and C. Joshi, "Experimental signatures of direct-laser-acceleration-assisted laser wakefield acceleration," *Plasma Phys. Control. Fusion*, vol. 60, no. 4, p. 044012, Apr. 2018.

[42] R. Lehe, M. Kirchen, I. A. Andriyash, B. B. Godfrey, and J.-L. Vay, "A spectral, quasi-cylindrical and dispersion-free Particle-In-Cell algorithm," *Comput. Phys. Commun.*, vol. 203, pp. 66–82, Jun. 2016.

[43] M. V. Ammosov, N. B. Delone, and V. P. Krainov, "Tunnel Ionization of Complex Atoms and Atomic Ions in Electromagnetic Field," in *Sov. Phys. JETP*, 1986, vol. 64, no. December 1986, p. 138.

[44] FBPIC contributors, "FBPIC Documentation," 2016. [Online]. Available: https://fbpic.github.io/. [Accessed: 26-Nov-2020].

[45] K. Schmid and L. Veisz, "Supersonic gas jets for laser-plasma experiments," *Rev. Sci. Instrum.*, vol. 83, no. 5, p. 053304, May 2012.

[46] J. P. Couperus *et al.*, "Tomographic characterization of gas-jet targets for laser wakefield acceleration," *Nucl. Instruments Methods Phys. Res. Sect. A Accel. Spectrometers, Detect. Assoc. Equip.*, vol. 830, pp. 504–509, Sep. 2016.

[47] L. Rovige *et al.*, "Optimization and stabilization of a kilohertz laser-plasma accelerator," *Phys. Plasmas*, vol. 28, no. 3, p. 033105, Mar. 2021.

[48] N. Lemos *et al.*, "Bremsstrahlung hard x-ray source driven by an electron beam from a self-modulated laser wakefield accelerator," *Plasma Phys. Control. Fusion*, vol. 60, no. 5, p. 054008, May 2018.